Nonlinear polarization rotation induced by ultrashort optical pulses in a semiconductor optical amplifier

Available online at www.sciencedirect.com
SCIENCE DIRECT®
Optics Communications 223 (2003) 169–179
OPTICS COMMUNICATIONS
www.elsevier.com/locate/optcom

Nonlinear polarization rotation induced by ultrashort optical pulses in a semiconductor optical amplifier

X. Yang[a,*], D. Lenstra[a,b], G.D. Khoe[a], H.J.S. Dorren[a]

[a] *Cobra Research Institute, Eindhoven University of Technology, P.O. Box 513, 5600 MB, Eindhoven, The Netherlands*
[b] *Division of Physics and Astronomy, Vrije Universiteit, FEW, De Boelelaan 1081, 1081 HV, Amsterdam, The Netherlands*

Received 24 January 2003; received in revised form 16 June 2003; accepted 17 June 2003

Abstract

We use a new rate-equation model for the propagation of sub-picosecond polarized optical pulses in a semiconductor optical amplifier (SOA). This model is based on the decomposition of the polarized optical field into TE and TM components that interact via the gain saturation, and accounts for two-photon absorption, free-carrier absorption, self- and cross-phase modulation, carrier heating, and spectral and spatial hole burning. For the first time, using our model, we have obtained numerical results for the nonlinear polarization rotation in pump–probe experiments with 200 fs pulses. These results are in good agreement with reported experimental measurements.

PACS: 42.55.P; 42.65.P; 42.65.R

Keywords: Semiconductor optical amplifier; Polarization rotation; Ultrafast switching

1. Introduction

Semiconductor optical amplifiers (SOAs) constitute important building blocks as nonlinear elements in all-optical signal processing applications. Most of the research work on optical switching has focused on employing SOA nonlinearities driven by inter-band transitions. However, the response time of these nonlinearities is restricted by the electron–hole recombination time, which is typically a few hundred picoseconds [1,2]. This response time fundamentally limits the processing speed of optical signal processing functionalities that are driven by inter-band transitions.

In order to obtain higher processing speeds, the use of SOA nonlinearities associated with intraband relaxation processes (i.e., carrier heating and cooling) have been suggested [2–8]. These nonlinearities are driven by two-photon absorption (TPA) and free carrier absorption (FCA), while the typical response time is restricted by the electron–electron and hole–hole interaction times, typically 50–100 fs. These ultrafast

* Corresponding author. Tel.: +3140247-2091; fax: +3140245-5197.
E-mail address: x.yang@tue.nl (X. Yang).

0030-4018/03/$ - see front matter
doi:10.1016/S0030-4018(03)01672-9

SOA nonlinearities could be employed for optical switching by placing the SOA into an interferometric arrangement [8].

An interesting alternative optical switching configuration can be realized through nonlinear polarization rotation in an SOA. Examples of optical switches based on this principle are published in [9–14], but a rate equation model capable of describing nonlinear polarization dynamics on sub-picosecond timescales is not yet available. In [14] a simple rate-equation model for nonlinear polarization rotation in an SOA is presented. This model works well up to speeds of a few gigahertz and its results are in excellent agreement with experimental data [14]. In the present paper, we extend our model for nonlinear polarization rotation in a semiconductor optical amplifier [14] by incorporating our results on the propagation of ultrashort pulses through an SOA [8]. This leads to a model that is capable of describing polarization dependent nonlinear gain saturation introduced by sub-picosecond optical pulses.

Similarly as in [14], the present model relies on the decomposition of the polarized optical field into TE and TM components. The TE and TM polarization eigenmodes have indirect interaction with each other via the gain saturation. SOAs with unstrained bulk active material have much larger TE amplification than TM, which is mainly due to the different confinement factors. Therefore, in practice, the SOA's active material is often tensile strained in order to enhance the TM gain with respect to TE so as to make the SOA approximately polarization independent. In this spirit, we account for different TE and TM gains by assuming that these polarizations couple to different hole reservoirs. This assumption is justified by the fact that in zinc-blende structures such as GaAs and InP the optical transitions occur between $j = 1/2$ type conduction band states and the $j = 3/2$ type valence band states, where the latter are subdivided into light-hole and heavy-hole band states. Two of the three possible transition types are selected by the TE and TM polarizations and they can be assigned two corresponding inversions, which are out of balance to an extent quantified by an empirical imbalance factor f [14].

In Section 2, we will extend the model of [14] to one that describes the polarization-dependent gain dynamics in an SOA on sub-picosecond timescales, fully in the spirit of, and using the pioneering results that are published in [3–5]. In Section 3, we will present simulation results that reveal gain dynamics induced by ultrashort optical pulses, and propose a schematic experimental setup that can be used for an optical switching device. We obtain the gain differences as well as the nonlinear phase shifts as a function of the control pulse energies. Our simulation results are in good agreement with the published experimental measurements, and for the first time, we show the simulation of the nonlinear phase shifts for pump–probe configuration. This paper is summarized in Section 4.

2. Model

We decompose the incoming arbitrarily polarized electric field in a component parallel to the layers in the waveguide (x component, TE-mode) and a perpendicular component (y component, TM mode). These two polarization directions are along the principal axes $(\hat{x}, \hat{y})$ that diagonalize the wave propagation in the SOA. In fact, apart from their indirect interaction through the carrier dynamics in the device, these two polarizations propagate independently from each other. We formulate a rate-equation model in the fashion of the one that is presented in [14], but extended to account for ultrafast nonlinear optical processes such as TPA, FCA, self-phase modulation (SPM), carrier heating, and spectral and spatial hole burning. The total electric field is defined by

$$E^{\mathrm{TE/TM}}(z,t) = \left[A^{\mathrm{TE}}(z,t)\hat{x} + A^{\mathrm{TM}}(z,t)\hat{y}\right] \mathrm{e}^{\mathrm{i}(\omega_0 t - k_0 z)} + c.c., \quad S^{\mathrm{TE/TM}}(z,t) = \left|A^{\mathrm{TE/TM}}(z,t)\right|^2, \tag{1}$$

where $k_0 = (n(\omega_0)/c)\omega_0$, $n(\omega_0)$ is the refractive index taken at the central frequency ω_0, c is the light velocity in vacuum, and $\hat{x}$ and $\hat{y}$ are unit vectors along the x and y directions. The frequency ω_0 has been chosen such

that the complex pulse amplitudes $A^{\mathrm{TE/TM}}(z,t)$ are slowly varying functions of z and t. The propagation equations for the TE and TM modes in the SOA are:

$$\left(\frac{\partial}{\partial z}+\frac{1}{v_g}\frac{\partial}{\partial t}\right)A^{\mathrm{TE}}(z,t)=\left\{\frac{1}{2}\Gamma^{\mathrm{TE}}(1+\mathrm{i}\alpha)g^{\mathrm{TE}}(z,t)-\frac{1}{2}\alpha_{\mathrm{int}}-\frac{1}{2}\Gamma_2\beta_2(1+\mathrm{i}\alpha_2)[S^{\mathrm{TE}}(z,t)+S^{\mathrm{TM}}(z,t)]\right.$$
$$\left.-\frac{1}{2}\Gamma^{\mathrm{TE}}\beta_c n_c(z,t)-\frac{1}{2}\Gamma^{\mathrm{TE}}\beta_v n_x(z,t)\right\}A^{\mathrm{TE}}(z,t), \tag{2}$$

$$\left(\frac{\partial}{\partial z}+\frac{1}{v_g}\frac{\partial}{\partial t}\right)A^{\mathrm{TM}}(z,t)=\left\{\frac{1}{2}\Gamma^{\mathrm{TM}}(1+\mathrm{i}\alpha)g^{\mathrm{TM}}(z,t)-\frac{1}{2}\alpha_{\mathrm{int}}-\frac{1}{2}\Gamma_2\beta_2(1+\mathrm{i}\alpha_2)[S^{\mathrm{TE}}(z,t)+S^{\mathrm{TM}}(z,t)]\right.$$
$$\left.-\frac{1}{2}\Gamma^{\mathrm{TM}}\beta_c n_c(z,t)-\frac{1}{2}\Gamma^{\mathrm{TM}}\beta_v n_y(z,t)\right\}A^{\mathrm{TM}}(z,t), \tag{3}$$

where the SOA parameters and their physical definitions are listed in Table 1. The first term on the right-hand side of Eqs. (2) and (3) represents the linear gain. α is the phase modulation parameter (or linewidth enhancement factor). The third term represents the TPA that is modeled by assuming that both the TE and TM modes are involved in the TPA process where α_2 is the corresponding phase modulation parameter, while the last two terms represent the FCA in the conduction and valence bands. We can reformulate Eqs. (2) and (3) in terms of equations for the intensities $S^{\mathrm{TE/TM}}$ and the phases $\phi^{\mathrm{TE/TM}}$, where the phase is defined as $A^{\mathrm{TE/TM}}(z,\tau)=\sqrt{S^{\mathrm{TE/TM}}(z,\tau)}\,\mathrm{e}^{\mathrm{i}\phi^{\mathrm{TE/TM}}}$ and

$$\frac{\partial S^{\mathrm{TE}}(z,\tau)}{\partial z}=[\Gamma^{\mathrm{TE}}g^{\mathrm{TE}}(z,\tau)-\alpha_{\mathrm{int}}-\Gamma^{\mathrm{TE}}\beta_c n_c(z,\tau)-\Gamma^{\mathrm{TE}}\beta_v n_x(z,\tau)]S^{\mathrm{TE}}(z,\tau)$$
$$-\Gamma_2\beta_2[S^{\mathrm{TE}}(z,\tau)+S^{\mathrm{TM}}(z,\tau)]S^{\mathrm{TE}}(z,\tau), \tag{4}$$

$$\frac{\partial\phi^{\mathrm{TE}}(z,\tau)}{\partial z}=\frac{1}{2}\alpha\Gamma^{\mathrm{TE}}g^{\mathrm{TE}}(z,\tau)-\frac{1}{2}\alpha_2\Gamma_2\beta_2[S^{\mathrm{TE}}(z,\tau)+S^{\mathrm{TM}}(z,\tau)], \tag{5}$$

$$\frac{\partial S^{\mathrm{TM}}(z,\tau)}{\partial z}=[\Gamma^{\mathrm{TM}}g^{\mathrm{TM}}(z,\tau)-\alpha_{\mathrm{int}}-\Gamma^{\mathrm{TM}}\beta_c n_c(z,\tau)-\Gamma^{\mathrm{TM}}\beta_v n_y(z,\tau)]S^{\mathrm{TM}}(z,\tau)$$
$$-\Gamma_2\beta_2[S^{\mathrm{TE}}(z,\tau)+S^{\mathrm{TM}}(z,\tau)]S^{\mathrm{TM}}(z,\tau), \tag{6}$$

Table 1
SOA parameter definitions and their values

Parameter	Symbol	Value	Units
Active volume	$V=L\times W\times D$	$250\times2\times0.1$	μm^3
Confinement factor	Γ^{TE}, Γ^{TM}, Γ_2	0.2, 0.14, 0.5	
Phase modulation coefficients	α, α_2	7, −1.5	
FCA coefficients	β_c, β_v	3×10^{-8},0	μm^{-1}
Electron–hole pair lifetime	τ_s	350	ps
Gain coefficient	$a^{\mathrm{TE}}(\omega_0)$, $a^{\mathrm{TM}}(\omega_0)$	2.5×10^{-5}	μm^3/ps
Group velocity	v_g	100	μm/ps
Internal loss	α_{int}	0.00175	μm^{-1}
Optical transition energies (conduction band)	E_c, E_{2c}	0.03, 0.7	eV
Optical transition energies (valence band)	E_v, E_{2v}	0.003, 0.07	eV
Carrier–carrier scattering times	τ_{1c}, τ_{1v}	0.1, 0.05	ps
Carrier–phonon relaxation times	τ_{1h}, τ_{hv}	0.7, 0.25	ps
TPA coefficient	β_2	9×10^{-7}	μm^2
Optical transition state density	N_0	3.6×10^6	μm^{-3}

$$\frac{\partial \phi^{\mathrm{TM}}(z,\tau)}{\partial z} = \frac{1}{2}\alpha \Gamma^{\mathrm{TM}} g^{\mathrm{TM}}(z,\tau) - \frac{1}{2}\alpha_2 \Gamma_2 \beta_2 [S^{\mathrm{TE}}(z,\tau) + S^{\mathrm{TM}}(z,\tau)]. \tag{7}$$

Here we have tacitly introduced a moving coordinate frame according to $\tau = t - z/v_{\mathrm{g}}$. The gains for TE/TM modes can be expressed as

$$g^{\mathrm{TE}}(z,\tau) = \frac{1}{v_{\mathrm{g}}} a^{\mathrm{TE}}(\omega_0)[n_{\mathrm{c}}(z,\tau) + n_x(z,\tau) - N_0], \tag{8}$$

$$g^{\mathrm{TM}}(z,\tau) = \frac{1}{v_{\mathrm{g}}} a^{\mathrm{TM}}(\omega_0)[n_{\mathrm{c}}(z,\tau) + n_y(z,\tau) - N_0], \tag{9}$$

where $a^{\mathrm{TE/TM}}(\omega_0)$ are the gain coefficients, $n_c(z,\tau)$, $n_x(z,\tau)$, and $n_y(z,\tau)$ represent the subset of electrons and holes, and N_0 the total number of states involved in the stimulated emission. The carrier densities satisfy

$$\begin{aligned}\frac{\partial n_{\mathrm{c}}(z,\tau)}{\partial \tau} = & -\frac{n_{\mathrm{c}}(z,\tau) - \bar{n}_{\mathrm{c}}(z,\tau)}{\tau_{1c}} - v_{\mathrm{g}} g^{\mathrm{TE}}(z,\tau) S^{\mathrm{TE}}(z,\tau) - v_{\mathrm{g}} g^{\mathrm{TM}}(z,\tau) S^{\mathrm{TM}}(z,\tau) \\ & - n_{\mathrm{c}}(z,\tau)\beta_{\mathrm{c}} v_{\mathrm{g}}[S^{\mathrm{TE}}(z,\tau) + S^{\mathrm{TM}}(z,\tau)],\end{aligned} \tag{10}$$

$$\frac{\partial n_x(z,\tau)}{\partial \tau} = -\frac{n_x(z,\tau) - \bar{n}_x(z,\tau)}{\tau_{1v}} - v_{\mathrm{g}} g^{\mathrm{TE}}(z,\tau) S^{\mathrm{TE}}(z,\tau) - n_x(z,\tau)\beta_{\mathrm{v}} v_{\mathrm{g}}[S^{\mathrm{TE}}(z,\tau) + S^{\mathrm{TM}}(z,\tau)], \tag{11}$$

$$\frac{\partial n_y(z,\tau)}{\partial \tau} = -\frac{n_y(z,\tau) - \bar{n}_y(z,\tau)}{\tau_{1v}} - v_{\mathrm{g}} g^{\mathrm{TM}}(z,\tau) S^{\mathrm{TM}}(z,\tau) - n_y(z,\tau)\beta_{\mathrm{v}} v_{\mathrm{g}}[S^{\mathrm{TE}}(z,\tau) + S^{\mathrm{TM}}(z,\tau)]. \tag{12}$$

The first terms on the right-hand sides of Eqs. (10)–(12) describe the relaxation of the electrons and holes to their quasi-equilibrium values $\bar{n}_i(z,\tau),\ i \in \{c,x,y\}$ that are specified later. These relaxation processes are driven by the electron–electron and hole–hole interactions with typically timescale 50–100 fs. The second terms describe the stimulated emission. It follows from Eq. (10) that for the electrons the TE and TM mode contribute equally to the stimulated emission, whereas, for the holes the TE-mode only involves $n_x(z,\tau)$ and the TM-mode only $n_y(z,\tau)$. This reflects our assumption that the TE mode and the TM mode couple to different reservoirs of holes [14].

Before the SOA model can be completed, we need formulate the equation for the total electron–hole pair density $N(z,\tau)$,

$$\frac{\partial N(z,\tau)}{\partial \tau} = \frac{I}{eV} - \frac{N}{\tau_s} - v_{\mathrm{g}}[g^{\mathrm{TE}}(z,\tau) S^{\mathrm{TE}}(z,\tau) + g^{\mathrm{TM}}(z,\tau) S^{\mathrm{TM}}(z,\tau)] + v_{\mathrm{g}}\beta_2 [S^{\mathrm{TE}}(z,\tau) + S^{\mathrm{TM}}(z,\tau)]^2, \tag{13}$$

where it is noted that $N(z,\tau)$ counts all the electron–hole pairs, including those that are not directly available for stimulated emission. The energy densities satisfy:

$$\begin{aligned}\frac{\partial U_{\mathrm{c}}(z,\tau)}{\partial \tau} = & \beta_{\mathrm{c}} \hbar \omega_0 n_{\mathrm{c}}(z,\tau) v_{\mathrm{g}}[S^{\mathrm{TE}}(z,\tau) + S^{\mathrm{TM}}(z,\tau)] - E_{\mathrm{c}} v_{\mathrm{g}}[g^{\mathrm{TE}}(z,\tau) S^{\mathrm{TE}}(z,\tau) + g^{\mathrm{TM}}(z,\tau) S^{\mathrm{TM}}(z,\tau)] \\ & + E_{2c} v_{\mathrm{g}} \beta_2 [S^{\mathrm{TE}}(z,\tau) + S^{\mathrm{TM}}(z,\tau)]^2 - \frac{U_{\mathrm{c}}(z,\tau) - \bar{U}_{\mathrm{c}}(z,\tau)}{\tau_{\mathrm{hc}}},\end{aligned} \tag{14}$$

$$\begin{aligned}\frac{\partial U_{\mathrm{v}}(z,\tau)}{\partial \tau} = & \beta_{\mathrm{v}} \hbar \omega_0 v_{\mathrm{g}}[n_x(z,\tau) + n_y(z,\tau)][S^{\mathrm{TE}}(z,\tau) + S^{\mathrm{TM}}(z,\tau)] - E_{\mathrm{v}} v_{\mathrm{g}}[g^{\mathrm{TE}}(z,\tau) S^{\mathrm{TE}}(z,\tau) \\ & + g^{\mathrm{TM}}(z,\tau) S^{\mathrm{TM}}(z,\tau)] + E_{2v} v_{\mathrm{g}} \beta_2 [S^{\mathrm{TE}}(z,\tau) + S^{\mathrm{TM}}(z,\tau)]^2 - \frac{U_{\mathrm{v}}(z,\tau) - \bar{U}_{\mathrm{v}}(z,\tau)}{\tau_{\mathrm{hv}}},\end{aligned} \tag{15}$$

where $U_c(z,\tau)$ represents the energy density in the conduction band and $U_v(z,\tau)$ the overall energy density in the valence band. In these equations the first terms describe the change in energy density due to the stimulated emission. The second terms describe the contribution of the FCA and the third terms account for the TPA. The last term represent the relaxation to equilibrium due to carrier–phonon interactions.

The total carrier density $N(z,\tau)$ and the total energy density $U_c(z,\tau)$ are needed to self-consistently calculate in each time-step the quasi-Fermi level $E_{fc}(z,\tau)$ and temperature $T_c(z,\tau)$ of the electrons, using

$$N(z,\tau)=\frac{1}{V}\sum_k F\left(E_{fc}(z,\tau),T_c(z,\tau),\frac{\hbar^2k^2}{2m_c^*}\right), \tag{16}$$

$$U_c(z,\tau)=\frac{1}{V}\sum_k \frac{\hbar^2k^2}{2m_c^*}F\left(E_{fv}(z,\tau),T_c(z,\tau),\frac{\hbar^2k^2}{2m_c^*}\right), \tag{17}$$

where $F(\mu,T,E)$ is the Fermi-Dirac distribution function defined as

$$F(\mu,T,E)=1/\left[1+\exp\left(\frac{E-\mu}{kT}\right)\right]. \tag{18}$$

Similarly, from $N(z,\tau)$ and $U_v(z,\tau)$, we can calculate the instantaneous Fermi levels and temperatures in the valence band using

$$N(z,\tau)=\frac{2}{V}\sum_k F\left(E_{fv}(z,\tau),T_v(z,\tau),\frac{\hbar^2k^2}{2m_v^*}\right), \tag{19}$$

$$U_v(z,\tau)=\frac{2}{V}\sum_k \frac{\hbar^2k^2}{2m_v^*}F\left(E_{fv}(z,\tau),T_v(z,\tau),\frac{\hbar^2k^2}{2m_v^*}\right), \tag{20}$$

where the factor of 2 on the right-hand side of Eqs. (19) and (20) is because two sub-bands are involved.

The quasi-equilibrium values $\bar{n}_i(z,\tau)$ are given by:

$$\bar{n}_c(z,\tau)=N_0F(E_{fc}(z,\tau),T_c(z,\tau),E_c), \tag{21}$$

$$\bar{n}_x(z,\tau)=f\bar{n}_y(z,\tau)=\frac{fN_0}{1+f}F(E_{fv}(z,\tau),T_v(z,\tau),E_v), \tag{22}$$

and the quasi-equilibrium values $\bar{U}_i(z,\tau)$ are

$$\bar{U}_c(z,\tau)=\frac{1}{V}\sum_k \frac{\hbar^2k^2}{2m_c^*}F\left(E_{fc}(z,\tau),T_L,\frac{\hbar^2k^2}{2m_c^*}\right), \tag{23}$$

$$\bar{U}_v(z,\tau)=\frac{1}{V}\sum_k \frac{\hbar^2k^2}{2m_v^*}F\left(E_{fv}(z,\tau),T_L,\frac{\hbar^2k^2}{2m_v^*}\right), \tag{24}$$

where T_L is the lattice temperature and f is the population imbalance factor describing the gain anisotropy introduced by tensile strain in the SOA. Eqs. (21) and (22) describe how the equilibrium populations $\bar{n}_x(z,\tau)$ and $\bar{n}_y(z,\tau)$ are clamped to each other as a consequence of tensile strain [14]. In case of unstrained bulk material, the gain will be isotropic and $f=1$. In case of tensile strain, TM gain will be larger than TE, i.e., $f<1$. For the energy relaxation, the temperature must be taken equal to the lattice temperature T_L (300 K).

We are aware of the fact that neglecting the gain and group velocity dispersion in our model for pulse propagation in an SOA limits the applicability of our model [15]. When the pulse duration is as short as

50–100 fs we can no longer expect good agreement between our model and measurements. However, in view of the apparently successful application of earlier models for pulses as short as 200 fs, we expect that the present model should be applicable for pulses of the same duration, especially when the central pulse frequency coincides with the gain maximum [3–5,8]. Using the gain curves of a commercially available JDS-Uniphase semiconductor optical amplifier, we have estimated that for an 800-μm long amplifier only minor changes occur in the pulse shape [16]. It should be remarked however, that this is no longer the case if the central pulse frequency is close to or at the zero gain region (at transparency). In this case large changes in the pulse shape take place, which could even lead to pulse break-up [19].

Moreover, we want to remark that we have modeled the phase-change by using a constant linewidth enhancement factor that is defined in the usual way [8,20]. Although this ignores dispersive effects due to strong variations in the carrier-density, such a treatment leads to result that are in agreement with experimental results.

Finally, we did not account for different group velocity dispersion coefficients for the TE and TM modes. It is shown in [21] that the difference in the group velocity between the TE and TM modes is in the order of 1%. We estimate that for a 500-μm long SOA, the pulse distortion effects remain less than 10%. This implies that for a not too long amplifier pulse pattern effects due to birefringence of the SOA are negligible.

3. Simulation results and discussion

The set of Eqs. (4)–(24) is solved numerically. The SOA length is 250 μm, and the active volume of 50 μm^3. Throughout this paper, we will consider optical pulses with Gaussian shape (200 fs, FWHM) as input. The SOA pump current is 120 mA. All other SOA parameters are listed in Table 1. The confinement factor Γ^{TM} is chosen to be 30% less than Γ^{TE} (see Table 1) [17,18]. The values for the gain coefficients $a^{TE/TM}(\omega_0) = 2.5 \times 10^{-5}$ μm^3/ps and the population imbalance factor $f = 0.9$ have been chosen in such a way that the small-signal amplification of the TE and TM mode are about 15 and 13 dB, respectively. A gain difference of 2 dB between the TE and the TM modes is typical for a JDS-Uniphase SOA at 120 mA [14].

It should be noted however that the SOA parameters N_0, $\Gamma^{TE/TM}$, $\alpha_{int}^{TE/TM}$, $v_g^{TE/TM}$ cannot be estimated accurately. We have solved this problem by compensating the combined uncertainties in these parameter values by assigning values to f and $a^{TE/TM}(\omega_0)$ in such a way that the SOA gain corresponds to typical values. In the simplest approach, one would choose $a^{TE}(\omega_0) = a^{TM}(\omega_0)$, which is correct in case of isotropic gain, whereas f can be estimated from the measured TE and TM amplification curves by using Eqs. (8), (9), (21), and (22). In this case the polarization-dependent gain could be totally explained by the band filling effects that are represented by the factor f. In a somewhat more complicated approach one can assume different values for $a^{TE}(\omega_0)$ and $a^{TM}(\omega_0)$. This latter approach was followed in [14] for a CW analyses.

The difficulties in estimating f and $a^{TE/TM}(\omega_0)$ may be inherent to our modeling the SOA strain in terms of the population imbalance factor f. In a more accurate, but also much more complicated model, one can calculate the band structure and transition matrix elements in the presence of tensile strain and keep track of the different optical transitions involved as well as the relevant populations. This would, however, extend beyond the scope of the present approach.

The TPA coefficient has been chosen in such a way that the SOA gain saturation is in agreement with experimental results presented in [19]. In Fig. 1, the SOA gain is presented as a function of the pulse energy. It follows from Fig. 1 that the net amplification becomes negative for pulse energies larger than 0.1 pJ. The curve presented in Fig. 1 is in quantitative agreement with experimental results presented in [19]. The net attenuation is due to the combined effects of TPA and FCA. It follows from Fig. 1 that for large pulse energies the difference in TE and TM gain almost vanishes, which can be explained by the fact that both modes equally contribute to the TPA. Thus for high energetic optical pulses the TPA terms in (4) and (6) will dominate.

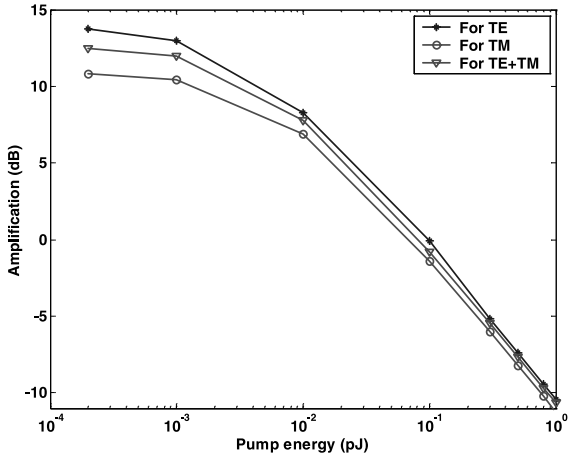

Fig. 1. Net amplification of the SOA as a function of the pump pulse energy, where the pulse width is 200 fs, and the pump is linearly polarized along the TE, the TM polarization axis or 45° with respect to the polarization axes of TE and TM modes (noted as TE + TM).

In Fig. 2, the gain recovery of the TE mode is presented at different positions in the SOA for a 1 pJ optical pulse. Due to the high pulse intensity, initially a strong change in the SOA gain takes place. Deeper in the SOA the pulse broadens. This is a result of the TPA, which attenuates the peak intensity in combination with the gain that amplifies both wings of the pulse. Note that the SOA gain initially recovers on a timescale of about half a picosecond.

The results that are presented so far characterize the SOA. In the following numerical experiments we investigate the feasibility of polarization switching using several pump–probe configurations. We will consider two 200 fs optical pulses that co-propagate through the SOA for two different situations. In the first case the pump pulse is either TE or TM polarized. In the second case the pump pulse is linearly polarized under an angle of 45° with the TE and TM polarization axes.

While the pulse travels through the SOA, not only the TE and TM field component intensities will be amplified (or attenuated), but also their phase difference will change. Hence, the state of polarization

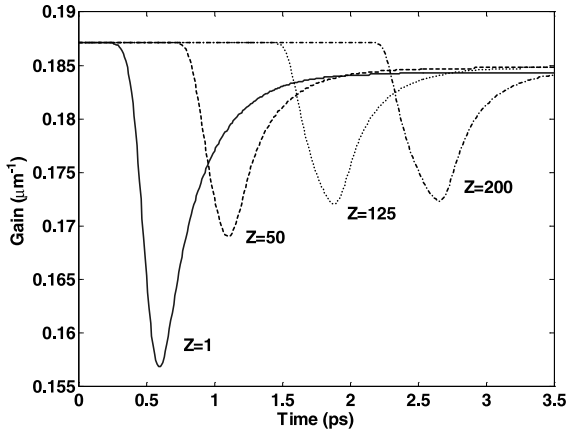

Fig. 2. Time variation of gain at different positions z (in μm) of the SOA, where the input pulse energies are 1 pJ with TE mode.

changes dynamically during the propagation of the pulse through the SOA. These processes are fully described in Eqs. (4)–(7).

The pump pulses have variable pulse energy. The probe pulse is linearly polarized (TE or TM) or under an angle of 45° with respect to the TE and TM polarization axes. The total probe pulse energy is fixed to 0.4 fJ. This small energy guarantees that the probe pulse propagate linearly through the SOA. The delay between the pump and probe pulses is optimized to be around 5 fs such that the latter propagates in the gain minimum introduced by the pump pulse.

In Fig. 3, the gain variations in the middle of the SOA ($z = 125$ μm) for the different polarization modes are presented. It can be observed that initially the SOA gains $g^{\mathrm{TE/TM}}$ are 0.187 and 0.208 μm^{-1} for the TE and TM modes, respectively, which is due to the imbalance factor $f = 0.9$. In Fig. 3(a), the TE gain is presented and in Fig. 3(b) the TM gain for different pump polarizations, where the pump pulse energy is 0.5 pJ. The results show that the largest decrease in the TE gain takes place if the pump pulse is also purely TE polarized and the smallest variation in the TE gain takes place if the pump pulse is purely TM polarized. A similar result holds for the TM gain. It can be noted from Fig. 3 that there is a clear gain compression induced by the strong pump pulses. After its compression, an initial gain recovery at a 0.5 ps timescale appears, then followed by a slow recovery time, which is associated with the inter-band effects determined by the electron and hole recombination times (350 ps in our cases, not shown in Fig. 3).

Because the gain temporarily decreases after the stimulated emission induced by the strong pump pulses, the probe pulse that follows will experience less amplification than when there is no pump pulse present. In Fig. 4 the relative amplitude differences are plotted for different pump and probe conditions. In Fig. 4(a), the amplification of the TE polarized probe pulse is shown as a function of pump pulse energy. Fig. 4(b) shows the similar result of TM polarized probe pulse. It follows from Fig. 4(a) that TE amplification is the smallest for TE pump, being reduced by about 20 dB when the pump pulse energy is 1 pJ. This amplification is about 0.5 dB larger if the pump pulse is linearly polarized under 45° and another 0.5 dB larger if the pump is TM polarized. Similar trends can be seen in Fig. 4(b), where the probe pulse is TM polarized. The corresponding phase shifts induced by the pump energies are plotted in Fig. 5. We find that the amplification and phase shifts are in good agreement with the experimental results in [20] for a TE polarized, 0.5 pJ pump pulse. In Fig. 5, we note that the phase shifts of TE polarized probe pulses are larger than TM probe pulses, which is due to the 2 dB small-signal amplification difference between TE and TM modes.

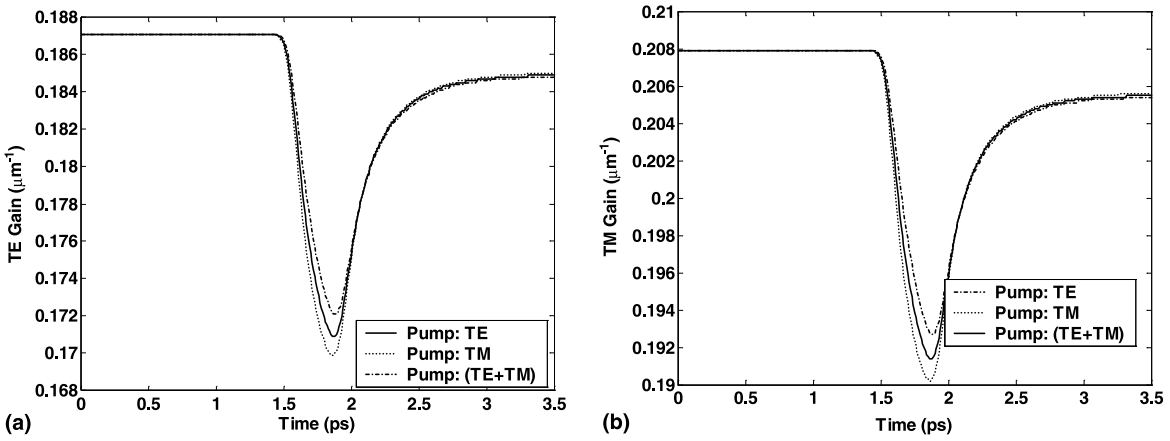

Fig. 3. Time variation of gain at the middle of SOA (at 125 μm), where the pump pulse energies are 0.5 pJ, and the pump pulse polarizations are the same as Fig. 1. In (a) the TE gain and in (b) the TM gain are shown.

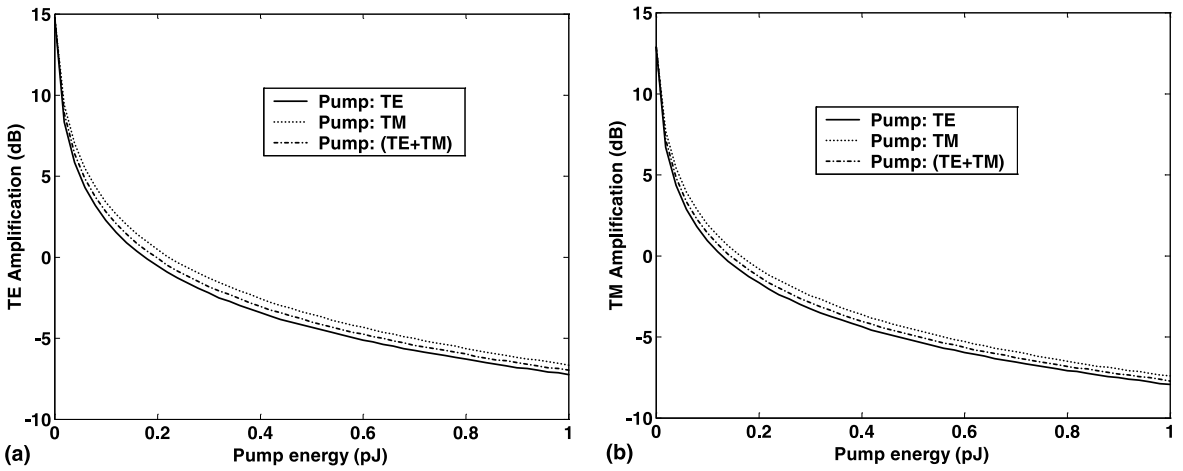

Fig. 4. Net amplification of the 0.4 fJ, 200 fs probe pulse as a function of the pump pulse energy, where the pump pulse polarizations are the same as Fig. 1. In (a), the TE amplification and in (b), the TM amplification are shown.

If the probe pulse is linearly polarized under an angle of 45° with respect to the TE and TM polarization axes, we can compare simultaneously the phase change for both of its TE and TM polarization components. The pump-induced phase shifts between TE and TM components of probe pulse as a function of pump energies and polarizations are shown in Fig. 6. If there is no pump pulse, we note that there is a constant phase shift, which is due to the intrinsic birefringence of the SOA when the current is 120 mA. The largest pump-induced phase shift of a TE polarized probe pulse is about 1 rad for all pump polarizations at pulse energy of 1 pJ. The phase shifts versus the pump–probe delay time is plotted in Fig. 7, where the probe pulse is TE polarized while pump pulse is TM polarized. Fig. 7 is in good qualitative agreement with the experimental result presented in [22], but the recovery timescale in the experiment is roughly twice as large as that of our simulation. However, in a very recent experiment, an exact faster recovery was obtained [23]. It will be subject of further research to investigate with our model which kind of recovery speeds may

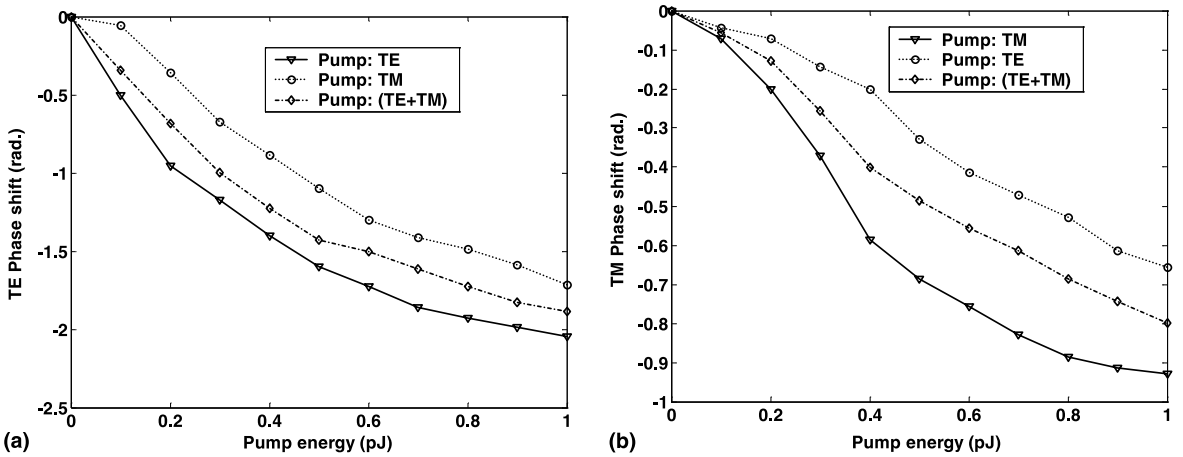

Fig. 5. Phase shifts of the 0.4 fJ, 200 fs probe pulse as function of pump pulse energies under the same conditions as in Fig. 4. In (a) the phase shift of TE component of probe pulse and in (b) the TM component of probe pulse are shown.

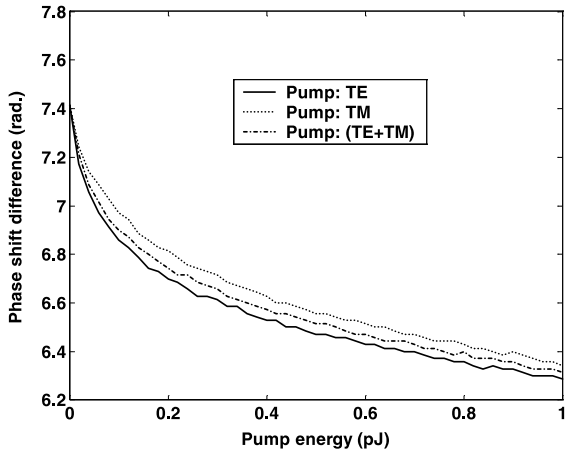

Fig. 6. Net phase shift difference $\Delta\phi$ between TE and TM modes ($\Delta\phi = \phi^{TE} - \phi^{TM}$) as function of pump pulse energy, where probe pulse polarizations are the same as Fig. 1.

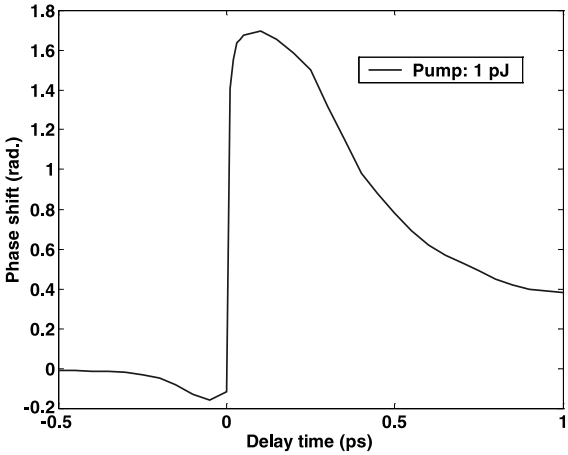

Fig. 7. Phase modulation of the probe pulse as function of pump–probe pulse delay time, where both of the probe and pump pulse are TE polarized.

be expected under various different conditions of SOA parameters. In any case, this kind of nonlinear phase difference forms the basis for polarization rotation in SOAs and can be exploited to construct all-optical ultrafast polarization switching devices [12].

4. Summary and conclusions

We have established a rate-equation model for sub-picosecond polarization-dependent pulses in a SOA. The model is based on the fact that the TE and TM eigenmode components have indirect interaction through the carriers. The model includes processes such as: TPA, FCA, self- and cross-phase modulation and carrier heating, and spectral and spatial hole burning. We have accounted for tensile strain by in-

troducing a population imbalance factor f [14]. Using this model, we can predict the ultrafast polarization rotation properties in an SOA.

For the parameters of a bulk JDS-Uniphase SOA, we presented simulation results for the amplitude and phase variations of 200 fs (FWHM) pulses. It is shown that the nonlinear phase shift difference between TE and TM modes is dependent on the pump–probe configurations. The nonlinear phase shift of a TE polarized probe pulse is more than 2 rad when the pump pulse energy is 1 pJ. In addition, the ultrafast phase shift between TE and TM polarization components of a probe pulse is about 1 rad when the pump energy is 1 pJ, which induces the nonlinear polarization rotation of the probe pulse.

Our model will help us to understand the polarization rotation effect in SOA induced by sub-picosecond pulses. The simulation results are in good agreement with published experimental results. Moreover, the ultrafast nonlinear polarization rotation in SOA can be employed in applications of all-optical terabit/s switching devices. Further experiments to verify these results are under way.

Acknowledgements

This work was supported by the Netherlands Organization for Scientific Research (NWO), the Netherlands Technology Foundation (STW) and the Technology Program of the Netherlands' Ministry of Economic Affairs through the ''NRC Photonics'', ''VIDI'' and ''Freeband TUC'' grants.

References

[1] R.J. Manning, A.D. Ellis, A.J. Poustie, K.J. Blow, J. Opt. Soc. Am. B 14 (1997) 3204.
[2] D. Cotter, R.J. Manning, K.J. Blow, A.D. Ellis, A.E. Kelly, D. Nesset, I.D. Phillips, A.J. Poustie, D.C. Rogers, Science 286 (1999) 1523.
[3] J. Mark, J. Mørk, Appl. Phys. Lett. 61 (1992) 2281.
[4] J. Mørk, J. Mark, C.P. Seltzer, Appl. Phys. Lett. 64 (1994) 2206.
[5] J. Mørk, M. Willatzen, J. Mark, M. Svendsen, C.P. Seltzer, Proc. SPIE (1994) 2146.
[6] M.Y. Hong, Y.H. Chang, A. Dienes, J.P. Heritage, P.J. Delfyett, IEEE J. Quant. Electron. 30 (1994) 1122.
[7] Y. Takahashi, A. Neogi, H. Kawaguchi, IEEE J. Quant. Electron. 34 (1998) 1660.
[8] H.J.S. Dorren, G.D. Khoe, D. Lenstra, Opt. Commun. 205 (2002) 247.
[9] H. Soto, D. Erasme, G. Guekos, IEEE Photon. Technol. Lett. 11 (1999) 970.
[10] H. Soto, D. Erasme, G. Guekos, IEEE Photon. Technol. Lett. 13 (2001) 335.
[11] T. Kakitsuka, Y. Shibata, M. Itoh, Y. Kadota, Y. Tohmori, Y. Yoshikuni, IEEE J. Quant. Electron. 38 (2002) 85.
[12] R.J. Manning, A. Antonopoulos, R. Le Roux, A.E. Kelly, Electron. Lett. 37 (2001) 229.
[13] R.P. Schreieck, M.H. Kwakernaak, H. Jackel, H. Melchior, IEEE J. Quant. Electron. 38 (2002) 1053.
[14] H.J.S. Dorren, D. Lenstra, Y. Liu, M.T. Hill, G.D. Khoe, IEEE J. Quant. Electron. 39 (2003) 141.
[15] M.Y. Hong, Y.H. Chang, A. Dienes, J.P. Heritage, P.J. Delfyett, Sol Dijaili, F.G. Patterson, IEEE. J. Select. Topics Quant. Electron. 2 (1996) 523.
[16] M.T. Hill, H. de Waardt, G.D. Khoe, H.J.S. Dorren, IEEE J. Quant. Electron. 37 (2001) 405.
[17] T.D. Visser, H. Blok, D. Lenstra, IEEE J. Quant. Electron. 35 (1999) 240.
[18] T.D. Visser, H. Blok, B. Demeulenaere, D. Lenstra, IEEE J. Quant. Electron. 33 (1997) 1763.
[19] F. Romstad, P. Borri, W. Langbein, J. Mørk, J.M. Hvam, IEEE Photon. Technol. Lett. 12 (2000) 1674.
[20] S. Bischoff, A. Buxens, St. Fischer, M. Dülk, A.T. Clausen, H.N. Poulsen, J. Mørk, Opt. Quant. Electron. 33 (2001) 907.
[21] T.D. Visser, H. Blok, D. Lenstra, IEEE J. Quant. Electron. 31 (1995) 1803.
[22] P. Borri, W. Langbein, J. Mørk, J.M. Hvam, Opt. Commun. 169 (1999) 317.
[23] H.J.S. Dorren, X. Yang, D. Lenstra, H. de Waardt, G.D. Khoe, T. Simoyama, H. Ishikawa, H. Kawashima, T. Hasama, IEEE Photon. Technol. Lett. 15 (2003) 792.